THE JOURNAL OF PHYSICAL CHEMISTRY C

Article

Cite This: J. Phys. Chem. C 2019, 123, 22725−22734

pubs.acs.org/JPCC

# Complex Garnets: Microscopic Parameters Characterizing Afterglow

Vasilii M. Khanin,[†,‡] Ivan I. Vrubel,[*,¶] Roman G. Polozkov,[¶] Ivan D. Venevtsev,[§] Piotr A. Rodnyi,[§] Tansu Tukhvatulina,[§] Kirill Chernenko,[∥] Winicjusz Drozdowski,[⊥] Marcin E. Witkowski,[⊥] Michal Makowski,[⊥] Evgenii V. Dorogin,[#] Nikolay V. Rudin,[#] Cees Ronda,[‡] Herfried Wieczorek,[‡] Jack Boerekamp,[‡] Sandra Spoor,[‡] Ivan A. Shelykh,[@,¶] and Andries Meijerink[†]

[†]Utrecht University, Princetonplein 5, 3584 CC Utrecht, The Netherlands

[‡]Philips Healthcare, High Tech Campus 4, 5656 AE Eindhoven, The Netherlands

[¶]ITMO University, Kronverksky 49, 197101 St. Petersburg, Russia

[§]Peter the Great St. Petersburg Polytechnic University, Polytekhnicheskaya 29, 195251 St. Petersburg, Russia

[∥]MAX IV Laboratory, Lund University, SE-22100 Lund, Sweden

[⊥]Faculty of Physics, Astronomy and Informatics, Nicolaus Copernicus University, Grudziadzka 5, 87-100 Torun, Poland

[#]STC YAFI, second Murinsky avenue 28, 194021 Saint-Petersburg, Russia

[@]Science Institute, University of Iceland, Dunhagi 3, IS-107 Reykjavik, Iceland

Supporting Information

**ABSTRACT:** Light yield, time response, afterglow, and thermoluminescence of Ce-doped garnet scintillators and persistent luminescent materials are controlled by a complex interplay between recombination and trapping/detrapping processes. Extensive research has contributed to a good qualitative understanding of how traps, impurities, and the presence of $Ce^{4+}$ affect the materials properties. In this work we present a quantitative model that can explain the thermoluminescence and afterglow behavior of complex garnets. In particular, the model allows the determination of capture rates and effective capture radii for electrons by traps and recombination centers in $Lu_1Gd_2Ga_3Al_2O_{12}$:Ce garnet ceramics. The model relies on solving a set of coupled rate equations describing charge carrier trapping and recombination in garnet ceramics doped with Ce and also codoped with a known concentration of an intentionally added electron trap, $Yb^{3+}$. The model is supported by analysis of a complete set of experimental data on afterglow, rise-time kinetics, and X-ray excited luminescence which show that thermoluminescence/afterglow are governed by trapping/detrapping processes following interactive kinetics with dominant recombination channel. The underlying reason for dominant recombination is the presence of a small fraction of $Ce^{4+}$ (≈2 ppm in the 0.2% Ce-doped sample) which have a very high capture cross section (≈2.7 Å effective radius) because of the Coulomb attractive nature of this recombination center. The quantitative insights on capture cross sections and concentrations of $Ce^{4+}$ help to better understand the optical properties of Ce-doped garnet scintillators and persistent luminescent materials and serve in optimizing synthesis procedures by tuning the $Ce^{3+}/Ce^{4+}$ ratio by codoping with divalent cations and annealing in an oxygen-containing atmosphere.

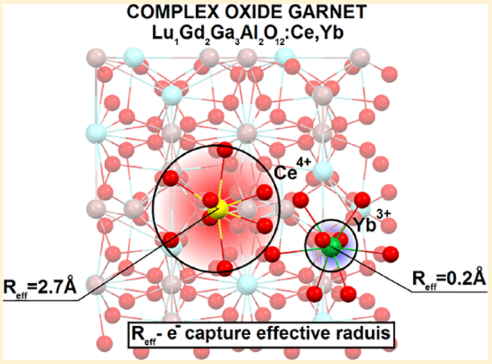


## INTRODUCTION

Complex Ce-doped garnets have received a lot of attention recently as promising scintillators for medical imaging,[1] phosphors for light-emitting diode applications,[2] and persistent phosphors.[3] The research on garnets generally consists of careful tuning of composition,[4] stoichiometry,[5] and impurity (doping) concentrations.[6] One of the main goals of these modifications is to influence the charge migration efficiency toward recombination or trapping sites, the so-called defect engineering.[7]

The presence of point defects acting as charge carrier traps in scintillating garnets leads to an undesired loss of light yield, high levels of afterglow, and presence of significant secondary decay components.[1] On the other hand, efficient trapping of the carriers is required for persistent luminescence garnets, so the synthesis procedures involve doping with additional impurities[8] or implementation of other methods[9,10] that can compete effectively with radiative recombination.

The competition between recombination, trapping, and retrapping of charge carriers is generally modeled using many-parameter systems involving rate equations.[11] These equations cannot be solved analytically, and suitable analysis generally

Received: May 30, 2019
Revised: August 14, 2019
Published: September 3, 2019






DOI: 10.1021/acs.jpcc.9b05169
J. Phys. Chem. C 2019, 123, 22725−22734

involves a set of simplifying assumptions.[12] Some of them, such as a dominance of a retrapping process or existence of a distribution of energy levels of the traps, can be deduced from systematic analysis of the experimental data on thermally stimulated luminescence (TSL), afterglow, or decay kinetics. Consequently, one can focus on the specific charge migration mechanisms, and the number of independent parameters characterizing the dynamics of the system can be substantially reduced.

Still, a quantitative and meaningful solution of the rate equations poses severe challenges.[13] Generally, in order to quantify the capture probabilities obtained from cross sections and other important trapping parameters, several complementing experiments are put together. Simultaneous measurement of thermally stimulated conductivity (TSC) and TSL is one of the common methods of trap parameter evaluation.[14,15] In particular, it can be used for the determination of the probability coefficients for recombination processes.[16] Correlation between the prominent TSL peaks and the derivative of the temperature dependence of the optical absorption of color centers is another technique regularly used to study the trap populations in dosimetry materials.[17]

In this work we estimate the charge carrier capture rates in $Lu_1Gd_2Ga_3Al_2O_{12}$:Ce garnet ceramics, annealed in oxygen atmosphere. The evaluation procedure consists of solving a system of rate equations which describe the competition between $Ce^{4+}$ ions and traps for the capture of conduction band (CB) electrons. The relevant parameters are defined from experimental data on TSL, afterglow, rise-time kinetics, and X-ray excited luminescence (XRL).

Additionally, by modification of doping levels for activator and traps in sintered samples, we have estimated the total trace concentration of $Ce^{4+}$ and effective radii of electron capture (from the CB) on $Ce^{4+}$ and $Yb^{3+}$ ions. The samples under study are $Lu_1Gd_2Ga_3Al_2O_{12}$:Ce ceramics with 0.001−1 mol % Ce doping (variation in recombination center (RC) concentration) and with 0.004 mol % Yb codoping (variation in specific trap concentration[18]).

## EXPERIMENTAL METHODS

Garnet ceramic samples of $Lu_1Gd_2Ga_3Al_2O_{12}$:Ce composition with 0.001−1 mol % Ce concentration were prepared at Philips Research, Eindhoven, by "mix-and-fire" sintering of 4 N purity oxides in air. An extra sample $Lu_1Gd_2Ga_3Al_2O_{12}$:Ce 0.2% was codoped with 40 mol ppm of Yb ions. The ceramics were sintered either in the form of pills of 14 mm diameter and 2 mm thickness (for afterglow and TSL glow curve measurements) or as rectangular sticks 20 × 4 × 4 mm (for rise-time and decay measurements). On the basis of X-ray diffraction patterns, it was concluded that all samples consist of a single garnet phase.

Afterglow curves were recorded together with XRL at room temperature (RT) in two time ranges in integral mode. Afterglow in the microsecond range was studied after 1.7 $\mu$s X-ray pulse (20 kV, 0.7 A, 1 cm distance, tungsten anode) and monitored with a Philips XQ2020 photomultiplier (PMT) and a Tektronix DPO2024 oscilloscope. Generally, to study the decay characteristics of scintillators either very short-term excitation (picosecond−nanosecond range) or very long excitations (on the order of seconds) are used. Consequently, the intermediate interval remains unexplored. In this work, we used an original setup with the source of rectangular X-ray pulses,[19] which allowed us to cover the microsecond−millisecond time range of scintillation decay.

XRL and afterglow in the range of seconds were detected after a 6 s X-ray pulse (120 kV, 100 mA, 20 cm distance, tungsten anode) with a Hamamatsu silicon photodiode and a Keithley M6485 picoammeter. All curves were normalized to the XRL signal intensity at the end of the irradiation pulse (assigned as $t = 0$).

Decay kinetics in a single-photon counting mode were measured under $\gamma$-quanta irradiation from an encapsulated 3 MBq $Na^{22}$ source, detected with a XQ2020 PMT on scintillator sticks covered by a reflector hood.

Measurements of rise (and decay) kinetics under 100 ps X-ray pulses were performed on scintillator sticks covered by a reflector hood at Delft University of Technology. Technical details of the experimental setup can be found in ref 20.

Photoluminescence emission spectra provided in this work were obtained with an UC-920 Edinburg Instruments spectrofluorimeter under 450 nm excitation from a Xe arc lamp. The equipment was calibrated to correct emission spectra for the sensitivity of the monochromators and PMTs.

XRL spectra were measured under continuous X-ray excitation (40 kV, 10 mA, 3 cm distance, tungsten anode). Emission spectra have been registered in a reflection geometry using a Lomo Photonica MDR-2 monochromator (1 nm resolution) coupled to a Hamamatsu H8259-01 photon-counting head. The spectra were corrected for the wavelength-dependent transmission of the monochromator and the spectral sensitivity of the PMT.

Afterglow spectra were measured at RT after 10 min of X-ray excitation in the setup for XRL spectra measurements.

TSL glow curves were measured in 80−550 K temperature range after irradiation of the samples with X-rays (40 kV, 10 mA, 3 cm distance, tungsten anode) at 80 K for 5 min. The detector was a Hamamatsu R6357 PMT, sensitive in the range of 200−900 nm. The waiting time between irradiation of the samples and the start of the measurements was 10 min. These TSL curves were recorded with $\beta = 0.25$ K/s heating rate.

Combination of XRL at low temperature with subsequent TSL measurements, the so-called ItTL measurements, had the following procedure. The sample was initially cooled down to 10 K and at this temperature was excited by the X-ray tube (45 kV, 5 mA, 15 cm distance, copper anode). During the irradiation (varied in the range of 3−40 min), the XRL integral intensity was measured. After the X-rays pulse the sample was kept at same 10 K for 60 min. The last step is heating up to 350 K with constant rate $\beta = 0.15$ K/s; this signal is measured as TSL. The detector was a Hamamatsu R928 PMT, sensitive in the range of 200−800 nm.

## EXPERIMENTAL RESULTS

In this section we present experimental results on decay kinetics under $\gamma$-quanta irradiation, XRL under steady excitation, afterglow measurements, and TSL. Comparison of the afterglow data obtained in the single-photon and steady-state excitation regimes justifies the processing of the X-ray irradiation as a number of independent X-ray photon absorptions. Afterglow spectra together with photoluminescence and XRL spectra allow to recognize $Ce^{3+/4+}$ ions as the primary radiative RC for direct and delayed luminescence. TSL and afterglow measurements show the existence of competition between RC and traps for charge carrier capture. ItTL measurements indicate that the majority of charge carriers



DOI: 10.1021/acs.jpcc.9b05169
J. Phys. Chem. C 2019, 123, 22725−22734

directly recombine on $Ce^{3+/4+}$ ions and do not get captured on traps.

**Comparison of Decay Kinetics in Single-Photon Counting Mode with Afterglow after an X-ray Pulse.** To investigate if the luminescence response to a large number of high-energy excitation events can be described by the sum of individual excitations, the luminescence time response for both cases has been measured.

The decay kinetics under gamma ray excitation (by a $Na^{22}$ $\gamma$-ray source) of $Lu_1Gd_2Ga_3Al_2O_{12}$:Ce 0.2% was measured in single-photon counting mode, black curve 2, Figure 1.

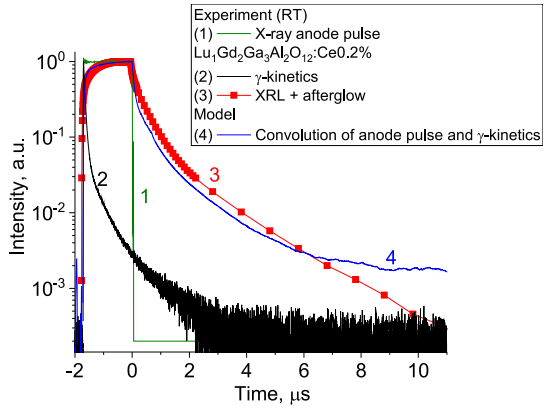


**Figure 1.** Green curve (1): profile of the X-ray excitation pulse. Black curve (2): decay kinetics obtained for $Lu_1Gd_2Ga_3Al_2O_{12}$:Ce 0.2% ceramics in single-photon counting mode. Red curve (3): XRL/afterglow signal obtained under rectangular X-ray excitation pulse. Blue curve (4): convolution of the excitation profile (1) with decay kinetics (2). Close similarity between curves 3 and 4 indicates a linear response of the sample to X-rays and allows to consider X-ray irradiation as absorption of independent X-ray photons.

Individual $\gamma$ rays excite the sample. The black curve 2 shows an initial fast decay with a ≈60 ns time constant that can be identified as the radiative decay time of the $Ce^{3+}$ emission. This is followed by a slower microsecond afterglow. The time response during and after a 1.7 $\mu$s X-ray pulse (pulse shape in green in Figure 1) is given by the red curve 3 in Figure 1 and shows a microsecond rise time during the pulse and also a microsecond afterglow. The decay of both kinetics and afterglow curve exhibits nonexponential behavior, which is due to trapping.[21]

Comparison of XRL and afterglow intensity (curve 3 in Figure 1) with a decay kinetics curve obtained under $Na^{22}$ $\gamma$-quanta irradiation (curve 2) reveals good alignment of these two curves. Indeed, performing the convolution of the rectangular excitation pulse (curve 1) with decay kinetics (curve 2) we get curve 4, in accordance with the following formula:

$$I_{lum}(t) = \int_{-\infty}^{t} I_{Exc}(\tau) I_K(t-\tau)\mathrm{d}\tau$$

$$= \begin{cases} I_{XRL}(t) = I_{Exc}\int_{-t_0}^{t} I_K(t-\tau)\mathrm{d}\tau,\ -t_0 \le t \le 0 \\ I_{Afterglow}(t) = I_{Exc}\int_{-t_0}^{0} I_K(t-\tau)\mathrm{d}\tau,\ t \ge 0 \end{cases} \quad (1)$$

$I_{Exc}(t)$ denotes the rectangular profile of the excitation pulse of the amplitude $I_{Exc}$ and duration $t_0$ = 1.7 $\mu$s (curve 1), $I_K(t)$ is the decay kinetics (curve 2). $I_{lum}(t)$ is the expected luminescence response (curve 4), which can be divided into the XRL part $I_{XRL}(t)$ for $t < 0$ and afterglow part $I_{Afterglow}(t)$ for $t > 0$.

The good match of the experimental curves obtained in continuous and single-photon modes indicates a linear response of the sample to X-rays and allows neglecting a potential accumulation of charge carriers in the traps and related memory effect[22] (refer to the Supporting Information for details). In the Modeling section we use this argument to process the continuous X-ray irradiation as absorption of a number of independent X-ray photons.

**$Ce^{3+/4+}$ as the Primary Luminescent Center.** To identify the primary recombination center, the XRL, afterglow, and photoluminescence spectra for the garnet samples have been measured.

The spectra are shown in Figure 2 and consist of a broad emission band around 560 nm that is typical of $Ce^{3+}$ 5d → 4f

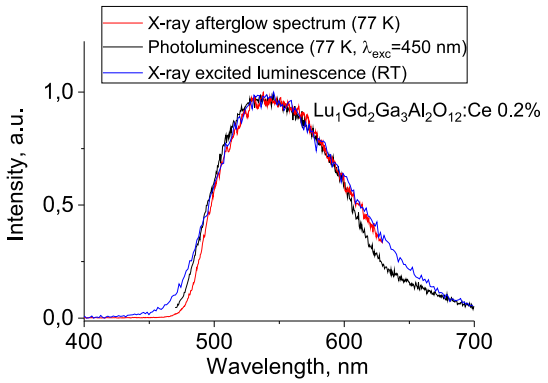


**Figure 2.** Red curve: afterglow emission spectrum (77 K) in the range of 1−10 min after X-ray irradiation. Black curve: photoluminescence spectrum (under 450 nm excitation, 77 K). Blue curve: XRL emission spectrum at RT. All spectra are recorded for the same $Lu_1Gd_2Ga_3Al_2O_{12}$:Ce 0.2% ceramics.

emission in garnets.[23] There are subtle differences in the spectra that may be related to generation of the emission at different depths in the crystal for the different excitation mechanisms. Reabsorption on the short-wavelength side where the emission overlaps with the $Ce^{3+}$ f → d absorption can slightly change the shape of the emission spectrum.

We suppose that $Ce^{3+}$ participates in thermoluminescence recombination process via the following mechanism:[24]

$$Ce^{3+} + \text{hole} \rightarrow Ce^{4+} \text{ (a)}$$

$$Ce^{4+} + e^{-} \rightarrow Ce^{3+*} \text{ (b)}$$

$$Ce^{3+*} \rightarrow \hbar\omega + Ce^{3+} \text{ (c)} \quad (2)$$

$Ce^{4+}$ (present in equilibrium state) can participate in recombination starting from stage b, thus leading to faster recombination.[25] Moreover, via such mechanism, $Ce^{4+}$ ions are efficient competitors to electron traps for capture of CB electrons.

**Competition between RC and Traps.** To study further the mechanism of the delayed luminescence, we investigated XRL and afterglow in the microsecond range for samples with Ce varying concentration in the range of 0.001−1%. The corresponding data are shown in Figure 3. For all samples the curves can be fitted by multiexponential decay law (for details



DOI: 10.1021/acs.jpcc.9b05169
J. Phys. Chem. C 2019, 123, 22725−22734

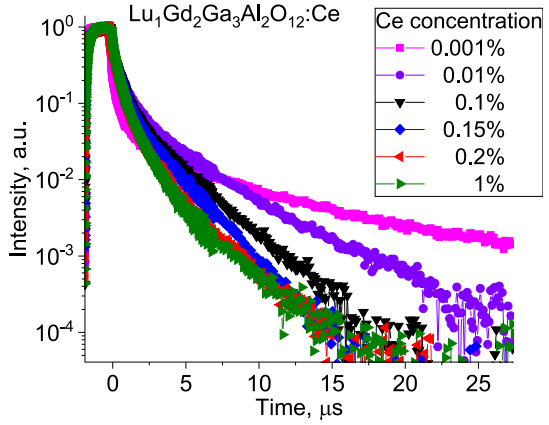


**Figure 3.** XRL and afterglow signal in the microsecond range for $Lu_1Gd_2Ga_3Al_2O_{12}$:Ce ceramics with Ce concentration varying in the range of 0.001−1%. The increased intensity of the secondary decay components with decreased Ce concentration indicates competition between traps and $Ce^{4+}$ ions for capture of charge carriers.

see the Supporting Information). The shortest decay component for all samples is about 60 ns, which is the typical radiative lifetime of the $Ce^{3+}$ 5d → 4f transition in garnets.[26,27] The slow-decay components are strongly dependent on Ce concentration. The systematic trend is that an increased Ce concentration results in the suppression of the integrated intensity of the secondary decay components (afterglow), which is due to competition between Ce ions and electron traps for capturing CB electrons.[28]

To obtain further insight into trapping of charge carriers for the garnet ceramics with different Ce concentrations, TSL glow curves were recorded after irradiation with X-rays (45 kV, 10 mA, 5 min). Also the intensity of the TSL signal is determined by competition between charge carrier trapping by Ce (giving direct emission) and by traps (giving afterglow/TSL). In Figure 4 the TSL glow curves are shown for all doping concentrations. The sample with the lowest Ce concentration shows the strongest TSL signal. $Lu_1Gd_2Ga_3Al_2O_{12}$:Ce TSL glow curve has a complex structure and consists of several TSL peaks: at 55, 250, 300, and 390 K. The low-temperature peak is a broad TSL structure that consists of several trap levels.[29] Usually the shallow traps are

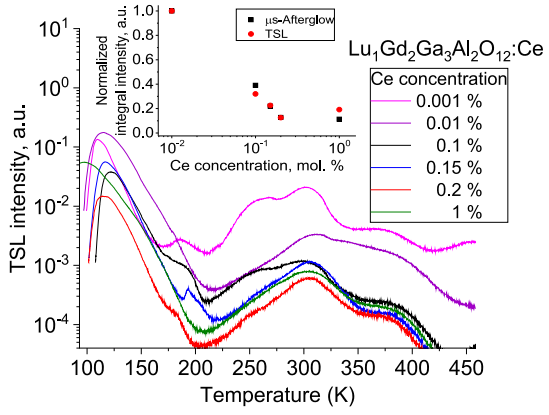


**Figure 4.** TSL glow curves for $Lu_1Gd_2Ga_3Al_2O_{12}$:Ce ceramics with Ce concentration varying in the range of 0.001−1%. The inset compares the integral intensities of TSL (200−400 K range) with secondary decays from Figure 3.

associated with the presence of structural defects,[21] e.g., cation antisites.[30] The deeper traps are related to impurities. In ref 31 we have shown that the 300 K TSL peak for $Gd_3Ga_3Al_2O_{12}$:Ce composition can be associated with Yb impurity, and the peak position barely shifts with Gd/Lu variation if Ga content is set to 60%. It has been repeatedly reported for various oxide garnets[8,32] that the two other TSL peaks on both sides of the Yb-related one are due to Cr (256 K for $Lu_1Gd_2Ga_3Al_2O_{12}$:Ce) and Ti or V (390 K) presence.

The main feature of Figure 4 is that the overall TSL intensity is proportionally lowered with higher Ce concentration. Moreover, the decreases in TSL (200−400 K) and afterglow (2−10 μs) integral intensities (Figure 3) are proportional to each other; see inset in Figure 4. From the similarity of the changes in secondary decay components and TSL intensities, we can attribute the secondary decay components (Figure 3) to delayed recombination on RC.

**Kinetic Order of the Thermoluminescence Process.** The kinetic order of the thermoluminescence process in garnets has been determined with TSL measurements performed with growing absorbed dose.

TSL glow curves for $Lu_1Gd_2Ga_3Al_2O_{12}$:Ce 0.2% ceramics are presented in Figure 5 for several values of X-ray irradiation

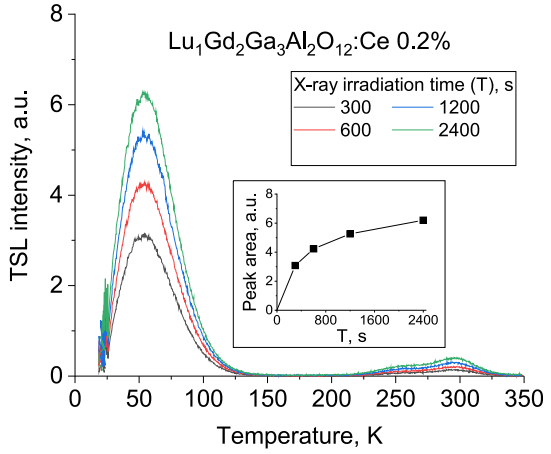


**Figure 5.** TSL glow curves (heating rate 0.15 K/s) for $Lu_1Gd_2Ga_3Al_2O_{12}$:Ce 0.2% ceramics after X-ray irradiation (40 kV, 5 mA, 200−2400 s). The integral intensity of peaks is saturated with increasing irradiation time, while peak maximum position and its shape remain the same for all excitation conditions. This is an unambiguous indicator for dominance of recombination channel in the samples under study.

duration. The area of the TSL peak at 55 K grows nonlinearly with increasing irradiation time, while the shape and position of the peak do not change. The inset in Figure 5 demonstrates the saturating behavior of the TSL peak integral intensity. These two observations indicate[11,33] that recombination dominates retrapping during the thermoluminescence response in the samples under study.

Having found the saturation dose for the TSL glow curves, we have diminished the X-ray irradiation dose in every other experiment provided in this work by at least 10 times, to decidedly stay away from saturation processes.

**Efficiency of CB Electron Capture by Traps and RC.** To study the efficiency of traps and RC to capture CB electrons, we used the ItTL measurements.



DOI: 10.1021/acs.jpcc.9b05169
J. Phys. Chem. C 2019, 123, 22725−22734

The competition between RC and traps for capture of CB electrons is determined by two main factors:[11] the capture probabilities for specific centers (traps or RC) and their concentrations; the latter can be tuned by doping. Here we use doping with $Yb^{3+}$ to introduce additional electron traps which can be identified in TSL glow curves. $Yb^{3+}$ is known[18] to serve as electron trap in Ce-doped garnets and gives rise to a peak around 300 K in garnets of the composition studied here.[34]

Figure 6 shows a comparison of the XRL intensity for nominally pure $Lu_1Gd_2Ga_3Al_2O_{12}$:Ce 0.2% ceramics and the

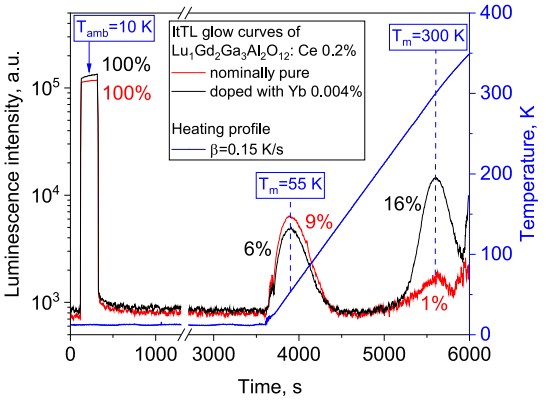


**Figure 6.** ItTL glow curves for $Lu_1Gd_2Ga_3Al_2O_{12}$:Ce 0.2% ceramics nominally pure (red curve) and codoped with 40 mol ppm Yb (black curve); see Experimental Methods section for details. The blue curve indicates the time dependence of the temperature. The rectangular signal at 200–400 s is the XRL intensity. Peaks at 4000 s ($T_m$ = 55 K) and 5600 s ($T_m$ = 300 K) are TSL glow peaks. The labeled % integral intensities are compared to the area under the XRL integral intensity (100%) to indicate the competition between traps and Ce ions for electron capture.

one codoped with 40 ppm Yb. The points marked at 300 s ($T$ = 10 K), 4000 s ($T_m$ = 55 K), and 5600 s ($T_m$ = 300 K) correspond to XRL, shallow, and deep traps TSL, respectively. Since irradiation is performed at a temperature where there is no thermal release of electrons to the conduction band, these three points approximately characterize the probabilities for direct capture of CB electrons by Ce ions or delayed by shallow and deep traps.

The experimental data in Figure 6 demonstrate that both samples under study have similar XRL integral intensities, which are taken as reference points corresponding to 100%. Very low luminescence intensity during the waiting period (300–3600 s) allows us to neglect emptying of traps via tunneling processes in later modeling.

The nominally pure and Yb-codoped samples have almost equal TSL integral intensity at 55 K (proportional to capture probability for shallow traps) of 6% and 9% of XRL, respectively. The codoped sample exhibits a significant increase of the 300 K TSL peak (16% compared to 1%) in Figure 6. The 300 K TSL peak in the $Lu_1Gd_2Ga_3Al_2O_{12}$:Ce 0.2% samples is caused by trace amounts of Yb ions which are a common impurity in the Lu source materials and are known to serve as deep electron traps.[18,34] By codoping the sample with 40 mol ppm of $Yb^{3+}$ ions, we enhance this TSL peak integral intensity by an order of magnitude.

The comparison of integral intensities for XRL and 55 K/300 K TSL peaks indicates a potential dominance of direct recombination at $Ce^{3+/4+}$ over trapping/retrapping at any of the electron traps in the sample doped with 0.2% of Ce. Still, also a significant fraction of the charge carriers is trapped, and this fraction can be enhanced by adding competing electron traps in rather low (ppm) concentrations.

**Trap Depth Distribution.** To determine the energy levels of the traps responsible for afterglow, we have analyzed the TSL data obtained with the use of preheating method.[12] The samples were repeatedly irradiated with the same dose, preheated up to a temperature $T_{stop}$ in the range of 15–300 K (only 15–125 K are shown for clarity), and then cooled down, and afterward TSL curves have been measured. In the recorded curves the shallowest TSL peak maximum ($T_{max}$) gradually shifts to higher temperatures with increase of $T_{stop}$ (see inset in Figure 7). Continuous distribution of the trap depths $E_t$ and depletion of progressively deeper traps[35] with increasing $T_{stop}$ explains this observed monotonous shift of the TSL peak maximum.

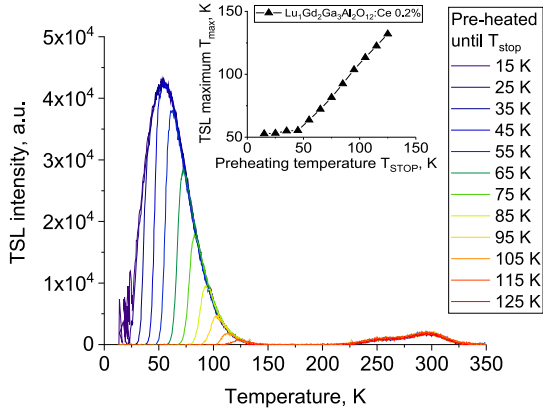


**Figure 7.** TSL glow curves for $Lu_1Gd_2Ga_3Al_2O_{12}$:Ce 0.2% ceramics measured with the preheating method for various values of $T_{stop}$. The inset depicts the shift of the position of TSL peak maxima ($T_{max}$) with increasing preheating temperature $T_{stop}$, which signifies the presence of the trap depth distribution.

Trap distribution in complex garnets has been experimentally studied in refs 3 and 9, and several mechanisms[36–39] can explain the underlying mechanism of the distribution. For more data about trap depth distribution, please refer to refs 34 and 35.

## MODELING

In this section we describe a mathematical model based on a system of rate equations, which we use to determine the capture rates and effective radii of the traps and RC. We discuss first the general simplifying assumptions about (de)trapping processes occurring in garnets, capitalizing on the experimental data reported in refs 2, 6, 7, 31, and 40–44. These simplifications are illustrated in Figure 8. We then describe the algorithm for the extraction of the model parameters from experimental afterglow, rise-time, and decay curves.

**Model.** In our mathematical model we account for the processes schematically shown in Figure 8. The corresponding set of the kinetic equations is given by system 3. The colors of the arrows in Figure 8 and the terms in eq 3 correspond to each other. The rate equations describe the simultaneous time evolution of the populations of the species involved in the processes giving rise to direct emission and TSL/afterglow:


DOI: 10.1021/acs.jpcc.9b05169
J. Phys. Chem. C 2019, 123, 22725–22734

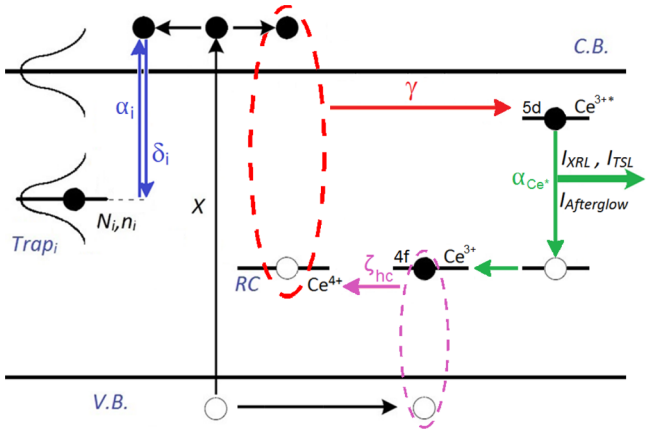


**Figure 8.** Band diagram describing the model of charge trapping and recombination. Free electrons in the CB and holes in the valence band (VB) are created by the absorption of a single gamma-quantum (process X) and then become localized on $Ce^{4+}$ or on traps. $Ce^{3+}$ ion has to capture VB hole first (becoming $Ce^{4+}$) to be able to participate in CB electron capture. The capture of electrons by $Ce^{4+}$ leads to creation of excited $Ce^{3+*}$ ions, which decay radiatively. Initial $Ce^{4+}$ concentration is later restored by leftover VB holes.

$$\begin{cases} \frac{dn_{cb}(t)}{dt} = \sum_i [\alpha_i n_i(t) - \delta_i n_{cb}(t)(N_i - n_i(t))] - \gamma n_{cb}(t) n_{Ce^{4+}}(t) \\ \frac{dn_i(t)}{dt} = -\alpha_i n_i(t) + \delta_i n_{cb}(t)(N_i - n_i(t)) \\ \dots \\ \frac{dn_{Ce*}(t)}{dt} = -\alpha_{Ce*} n_{Ce*}(t) + \gamma n_{cb}(t) n_{Ce^{4+}}(t) \\ \frac{dn_{Ce^{3+}}(t)}{dt} = \alpha_{Ce*} n_{Ce*}(t) - \zeta_{hc} n_{holes}(t) n_{Ce^{3+}}(t) \\ \frac{dn_{Ce^{4+}}(t)}{dt} = +\zeta_{hc} n_{holes}(t) n_{Ce^{3+}}(t) - \gamma n_{cb}(t) n_{Ce^{4+}}(t) \\ \frac{dn_{holes}(t)}{dt} = -\zeta_{hc} n_{holes}(t) n_{Ce^{3+}}(t) \end{cases} \quad (3)$$

where $n_{cb}$, $n_i$, and $n_{holes}$ ($cm^{-3}$) are concentrations of electrons in conduction band and on traps and holes in valence band, respectively; $n_{Ce^{3+}}$, $n_{Ce*}$, $n_{Ce^{4+}}$ ($cm^{-3}$) are concentrations of Ce ions in the ground, excited, and ionized states, respectively; $i$ is the index for electron trap with detrapping time ($\tau_i = 1/(\alpha_i)$), where $\alpha_i$ ($s^{-1}$) is the detrapping rate; $\delta_i$, $\gamma$, and $\zeta_{hc}$ ($cm^3\ s^{-1}$) are the capture probability coefficients for electron traps, $Ce^{4+}$ and $Ce^{3+}$, respectively; $N_i$ ($cm^{-3}$) is the total concentration of trap $i$; $\alpha_{Ce*}$ ($s^{-1}$) is the radiative decay rate of the $Ce^{3+}$ 5d → 4f transition.

Writing eq 3 we have accounted for the following processes, illustrated in Figure 8. Electrons in the conduction band and holes in the valence band are generated initially by absorption of a single X-ray photon (process X). Then free carriers rapidly thermalize and become captured by specific centers: electrons localize at various types of traps (blue arrow down) and $Ce^{4+}$ ions (red arrows); holes are captured by $Ce^{3+}$ ions (violet arrows). The rates of these processes are defined by the respective capture probability coefficients $\delta_i$, $\gamma$, and $\zeta_{hc}$. The electrons captured on traps can be released to the CB with the rate $\alpha_i$ (blue arrow up). Free electrons can again be recaptured by any traps or $Ce^{4+}$ ions.

Important notion is that we consider $Ce^{4+}$ ions as the only RC that captures CB electrons.[24]

The thermal trap depth ($E_t$) in our model is distributed over a band of varying depths and is characterized by an array of detrapping rates ($\alpha_i$). The capture of electrons by RCs ($Ce^{4+}$) leads solely to radiative recombination (thermal ionization of $Ce^{3+*}$ $5d_1$ excited state is neglected). The emission is schematically shown by the green arrow of XRL ($I_{XRL}$), afterglow ($I_{Afterglow}$), or TSL ($I_{TSL}$) signal in Figure 8.

Note that we use the system of ordinary, not partial, differential equations for the description of the kinetics of the system, thus neglecting the diffusion of the electrons and holes from the ionization track of an X-ray photon. This simplification is due to the presence of a large (compared to the number of holes generated by a single X-ray photon absorption) equilibrium concentration of $Ce^{4+}$ ions, $n_{Ce^{4+}}$. For more details on disregard of diffusion and $Ce^{4+}$ concentration estimations, refer to the Supporting Information.

The feasibility of neglecting diffusion terms is also provided by the experimental observation that luminescence is qualitatively the same in single-photon counting mode and in the regime of spatially homogeneous X-ray irradiation; see the Experimental Results section.

**Simplifications and Initial Conditions.** The system of equations proposed in the previous section can be significantly simplified if one accounts for the experimental results both in this work and in refs 2, 6, 7, 31, and 40−44.

The works show that even a trace amount of $Ce^{4+}$ ions due to Mg,[45] Ca[46] codoping or oxygen annealing of garnets[24] significantly reduces thermoluminescence[47] and speeds up the rise-time kinetics.[25] Simple estimations (provided in the Supporting Information) show that 1−2 ppm concentration of charge-compensated $Ce^{4+}$ ions creates larger presence of RC centers compared to $Ce^{3+}$ capturing valence band holes (generated by single X-ray photon). We write this condition in the following way:

$$\begin{cases} n_{holes} \ll n_{Ce^{4+}}^{equilibrium}|_{t=0} \\ n_{Ce^{4+}}^{equilibrium}|_{t=0} \ll n_{Ce^{3+}} \end{cases} \quad (4)$$

These conditions allow to neglect holes transport and carrier diffusion, and as a consequence we consider the kinetic equations homogeneous. Neglecting hole transport is equivalent to $\zeta_{hc} \to \infty$.

We can now write charge neutrality ($n_{electrons} = n_{holes}$) of a scintillation volume in the following form:

$$\begin{aligned} n_{Ce^{4+}}(t) &= n_{Ce^{4+}}^{equilibrium} + n_{holes}(t) \\ &= n_{Ce^{4+}}^{equilibrium} + n_{cb}(t) + \sum_i n_i(t) \end{aligned} \quad (5)$$

Implementing the simplifications to eq 3 we derive the equations system for modeling as eq 6.

$$\begin{cases} \frac{dn_{cb}(t)}{dt} = \sum_i [\alpha_i n_i(t) - \delta_i n_{cb}(t)(N_i - n_i(t))] - \gamma n_{cb}(t) n_{Ce^{4+}}(t) \\ \frac{dn_i(t)}{dt} = -\alpha_i n_i(t) + \delta_i n_{cb}(t)(N_i - n_i(t)) \\ \dots \\ \frac{dn_{Ce*}(t)}{dt} = -\alpha_{Ce*} n_{Ce*}(t) + \gamma n_{cb}(t)(n_{Ce^{4+}}^{equilibrium} + n_{cb}(t) + \sum_i n_i(t)) \end{cases} \quad (6)$$

Equation 6 is a version of the standard rate equations describing the trapping dynamics[11,48] with an additional term accounting for the presence of charge-compensated $Ce^{4+}$ ($n_{Ce^{4+}}$) ions discussed above.

We treat this system of equations numerically as a Cauchy problem for electron populations $n_i(t)$, $n_{cb}(t)$, and $n_{Ce^{4+}}(t)$. In the presented model we define $\alpha_i = 1/(\tau_i)$, $i$ = (1:35), as an


DOI: 10.1021/acs.jpcc.9b05169
J. Phys. Chem. C 2019, 123, 22725−22734

array of detrapping rates (inverse values to distribution of detrapping times $\tau_i$ in the range from $10^{-7}$ to $10^5$ s).

Initially all traps and $(Ce^{3+})^*$ ions are assumed to be empty, $n_{Ce^*}(t = 0) = 0$ and $n_i(t = 0) = 0$ for all $i$. The only nonzero initial value is given to the electron population in the conduction band ($X_{ion} \approx 10^{16}$ cm$^{-3}$) appearing due to the absorption of a single 50 keV gamma-quantum which triggers luminescence. As luminescence in our system is provided by the 5d → 4f transition of $Ce^{3+}$* ions, the luminescence decay curve corresponding to the black curve in Figure 1 is given by

$$I_{lum}(t) = \alpha_{Ce^*} n_{Ce^*}(t) = \frac{1}{\tau_{Ce^*}} n_{Ce^*}(t) \quad (7)$$

where the transition rate $\alpha_{Ce^*}$ corresponds to ≈1/60 ns$^{-1}$. The shape of the afterglow and XRL curves can be then computed according to the eq 1.

**Model Calibration and Fitting Procedure.** The fitting procedure includes three steps which are performed in a self-consistent manner. The initial values of the parameters are approximated from general considerations. For example, the starting value for $\gamma \cdot n_{Ce^{4+}}$ ($Ce^{4+}$ capture rate) is adopted as $10^9$ (s$^{-1}$) (an inverse value to typical rise-time constant observed for Ce-doped garnets[25]). The initial concentration of $Ce^{4+}$ is put as 0.1% of total Ce concentration (2 ppm of $Ce^{4+}$ in the $Lu_1Gd_2Ga_3Al_2O_{12}$:Ce 0.2% reference sample).

The relative values $\delta_i \cdot N_i$ and $\gamma \cdot n_{Ce^{4+}}$ are determined by an iterative procedure of the simultaneous convergence of modeled and experimentally measured decay kinetics, XRL, and afterglow curves in the whole range of experimentally observed time interval. The process is stopped when a proportional variation of all the $\delta_i \cdot N_i$ and $\gamma \cdot n_{Ce^{4+}}$ coefficients does not significantly influence the modeled XRL and afterglow/decay curves shape (see the Supporting Information). In the second step we define the absolute values of $\delta_i \cdot N_i$ and $\gamma \cdot n_{Ce^{4+}}$ coefficients simultaneously, converging the computed and experimentally measured rise kinetics, which reflects the rate of electron capturing on recombination centers and traps. The modeling of rise-time kinetics is very sensitive to the values of $\delta_i \cdot N_i$ and $\gamma \cdot n_{Ce^{4+}}$ coefficients. In Figure 9 the rise-part of the kinetics for $Lu_1Gd_2Ga_3Al_2O_{12}$:Ce 0.2% is shown compared to three different fits. The rising edge of the scintillation flash is significantly over- or underestimated when inadequate $\delta_i \cdot N_i$ and $\gamma \cdot n_{Ce^{4+}}$ absolute values are used.

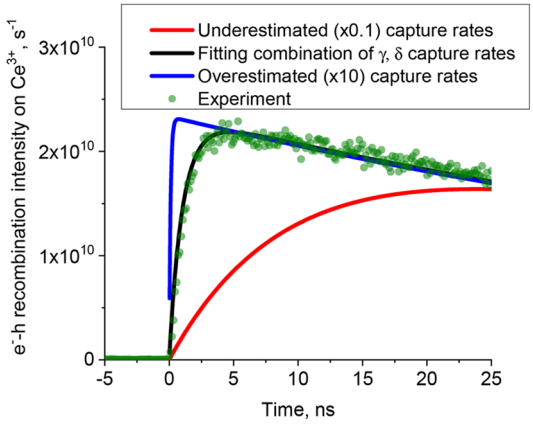


**Figure 9.** Experimental and modeled rising edge of $Lu_1Gd_2Ga_3Al_2O_{12}$:Ce 0.2% kinetics. The modeled kinetics is obtained with the final (×1) and ×0.1; ×10 coefficients for charge capture.

The third step is the separation of $\delta_i$ and $\gamma$ (cm$^3$ s$^{-1}$) probability coefficients from concentrations of the traps $N_i$ and $Ce^{4+}$ ions $n_{Ce^{4+}}$, respectively. For this we use the afterglow data obtained for the samples with varying concentrations of Ce (RC) and specific impurities (Yb-related traps).

The traps capture probability coefficients $\delta_i$ can be estimated only for the cases of impurity-related traps. Assuming that the total concentration of Yb-related traps $N_{i=Yb}$ is equal to the total amount of Yb ions ($N_{Yb}$ = 40 mol ppm of Yb ions), we directly get $\delta_{Yb}$ from $\delta_i \cdot N_i$ corresponding to the reference $Lu_1Gd_2Ga_3Al_2O_{12}$:Ce 0.2%,Yb 0.004% sample.

To determine the initial concentration of $Ce^{4+}$ ions, we varied the Ce concentration in the samples under study, assuming that the initial concentration of $Ce^{4+}$ ions is proportional to the total Ce concentration. We have observed a proportional decrease of TSL and afterglow intensities (Figure 3 and Figure 4) with increased Ce doping (section 3.3). The initial concentration of $Ce^{4+}$ can then be determined from the simultaneous fits of experimental afterglow curves.

Examples of fits are provided in the Supporting Information.

## DISCUSSION

**Capture Rates for Traps and $Ce^{4+}$.** The obtained numerical values of the parameters characterizing the luminescence kinetics for our samples are summarized in Table 1. The primary capture centers, which are $Ce^{4+}$, the shallow trap (typical lifetime $\tau$ = 0.3 μs), and Yb-related trap (typical lifetime 1−$10^3$ s) have rates of 4 × $10^8$, 1 × $10^8$, and 2 × $10^7$ s$^{-1}$, respectively. The capture rate of $Ce^{4+}$ is half an order of magnitude larger than the capture rates for any electron trap.

**Table 1. Capture Rates of Traps and RC ($Ce^{4+}$) in Nominal Pure and Codoped with 40 mol ppm Yb $Lu_1Gd_2Ga_3Al_2O_{12}$:Ce 0.2% Ceramics**

| | nominally pure ceramics | | Yb codoped ceramics | |
|---|---|---|---|---|
| capture center | rate, s$^{-1}$ | concn, cm$^{-3}$ | rate, s$^{-1}$ | concn, cm$^{-3}$ |
| $Ce^{4+}$ ion | $\gamma \cdot n_{Ce^{4+}}$ = 4 × $10^8$ | $n_{Ce^{4+}}$ = 3 × $10^{16}$ | $\gamma \cdot n_{Ce^{4+}}$ = 4 × $10^8$ | $n_{Ce^{4+}}$ = 3 × $10^{16}$ |
| structural defects ($i$ = 2, $\tau_2$ = 0.3 μs) | $\delta_2 \cdot n_2$ = 1 × $10^8$ | $n_2 \approx 10^{18}$[a] | $\delta_2 \cdot n_2$ = 1 × $10^8$ | $n_2 \approx 10^{18}$[a] |
| impurity-related ($Yb^{3+}$) | $\delta_{Yb} \cdot n_{Yb}$ = 1 × $10^6$ | $n_{Yb}$ = 2 × $10^{16}$ | $\delta_{Yb} \cdot n_{Yb}$ = 2.5 × $10^7$ | $n_{Yb}$ = 5 × $10^{17}$ |

[a]Assuming traps Coulomb neutrality.

More data on electron capture rates for two $Lu_1Gd_2Ga_3Al_2O_{12}$:Ce 0.2% ceramics with and without Yb codoping are presented in Figure 10, in which the $x$-axis represents the distribution of traps lifetime $\tau_i = 1/(\alpha_i)$ (s) and the $y$-axis corresponds to the distribution of the traps capture rates $\delta_i \cdot N_i$. The red and black curves correspond to the nominally pure and Yb-codoped samples, respectively. It can be clearly seen that 40 mol ppm Yb codoping increases the values of $\delta_i N_i$ for $i$ = 20−30, while other trap capture rates are nearly the same for both samples.

We have also plotted the $\gamma n_{Ce^{4+}}$ (s$^{-1}$) capture rate for recombination centers to show that $\gamma n_{Ce^{4+}}$ values dominate over $\delta_i N_i$ capture rates of $i$-traps. Note that the reference value of the rate $\gamma n_{Ce^{4+}}$ (s$^{-1}$) capture rate is 4 times higher than $\delta_i N_i$


DOI: 10.1021/acs.jpcc.9b05169
J. Phys. Chem. C 2019, 123, 22725−22734

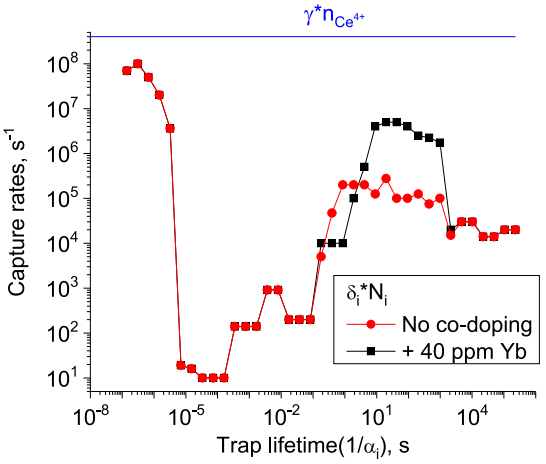


**Figure 10.** Distribution of electron capture rates $\delta_i \cdot N_i$ on $i$-traps for nominally pure $Lu_1Gd_2Ga_3Al_2O_{12}$:Ce 0.2% ceramics (red curve) and ceramics codoped with 40 ppm Yb (black curve). Capture rate for $Ce^{4+}$ $\gamma n_{Ce^{4+}}$ (blue line) is added for clarity, to show that it dominates over the traps capture rates.

capture rates of all $i$-traps. This result is in agreement with conclusions drawn from experimental TSL data in the Experimental Results section, that the thermoluminescence processes in our ceramics have a dominating character in recombination channel.[11]

The underlying reason for the dominance is the presence of initial $Ce^{4+}$ concentration in ceramics, annealed in oxygen-rich atmosphere. We estimate (Table 1) that the sample $Lu_1Gd_2Ga_3Al_2O_{12}$:Ce 0.2% Ce has 2 ppm of $Ce^{4+}$ ions ($3 \times 10^{16}$ $cm^{-3}$), which provide a significant number of sites ready for recombination with CB electrons ($n_{cb}$).

In principle, the knowledge of capture rates and recombination probability from Figure 10 is enough to simulate not only afterglow curves but also TSL glow curves. We have attempted modeling the TSL glow curves with the obtained set of parameters (not shown) and found out that while the TSL peak positions and shapes are well predicted, the TSL intensity can be several times off. We suppose that the reason is in temperature dependence for charge carrier distribution over trapping centers; for details please see the Supporting Information.

**5.2. Effective Radii of Capture Centers.** To generalize the results presented in the previous section we have also calculated capture cross sections for electrons by $Ce^{4+}$ RC and $Yb^{3+}$ ions (traps), which play a major role in kinetics. These parameters can be calculated from capture probability coefficients semiclassically. Assuming that an electron moves chaotically due to thermal fluctuations in the disorder of the solid solution, we can consider the capture rates as probability of the capture center with cross section $\sigma$ to be crossed by an electron trajectory per time unit, which can be expressed as[13]

$$\delta_i = \sigma_i \cdot \upsilon_{el},\ \gamma = \sigma_{RC} \cdot \upsilon_{el} \tag{8}$$

where $\upsilon_{el}$ is the velocity of the thermalized electron; $\gamma$ and $\delta_i$ are the capture probability coefficients for $Ce^{4+}$ and $i$-traps, respectively; $\sigma_{RC}$ and $\sigma_i$ are the capture cross sections for $Ce^{4+}$ and $i$-traps, respectively.

From the band structure plot provided in ref 49, we estimate the effective mass of an electron to be $m^* \approx 2m_e$ in garnets. Then the thermal electron velocity at RT is equal to $\upsilon_{el} = 7 \times 10^6$ $cm \cdot s^{-1}$. Since the concentration of $Ce^{4+}$ ions has been obtained above, we can immediately calculate the effective radii of the recombination centers as

$$r_{RC} = \sqrt{\frac{\gamma}{\pi \upsilon_{el}}} = 2.7\ \text{Å} \tag{9}$$

$Ce^{4+}$ ions in a garnet lattice with trivalent cations behave as Coulomb attractive centers for electrons with effective radius $r_{RC} = 2.7$ Å (and typical cross section[13] $\sigma = 2 \times 10^{-15}$ $cm^2$).

The effective radius for Yb traps can be obtained by considering a nominal Yb-codoping concentration of $5 \times 10^{17}$ $cm^{-3}$ (40 mol ppm of Yb ions), assuming that all $Yb^{3+}$ ions are incorporated in the garnet lattice:

$$r_{Yb} = \sqrt{\frac{\delta_{Yb}}{\pi \upsilon_{el}}} = 0.2\ \text{Å} \tag{10}$$

The calculated value of effective radius (close to Bohr radius) is fitting well into reasoning that $Yb^{3+}$ ions behave as neutral traps in garnet lattice.[18]

## CONCLUSIONS

Analysis of extensive experimental data on X-ray luminescence, afterglow, thermoluminescence, and rise and decay kinetics under pulsed X-ray and gamma-ray excitation of a Ce-doped ceramic garnet scintillator ($Lu_1Gd_2Ga_3Al_2O_{12}$) has been performed using a rate equation model describing charge carrier trapping/detrapping and recombination. To obtain a better quantitative understanding, the Ce concentration was varied (0.001−1%), and also a codoped ceramic with 0.2% Ce and 40 mol ppm of $Yb^{3+}$ (a known electron trap) was investigated. It was demonstrated that the trapping/detrapping processes are governed by interactive kinetics with high recombination probability. Calculations based on the model provide quantitative information on electron-trapping rates and concentrations of intrinsic trapping centers, $Yb^{3+}$ and $Ce^{4+}$.

The calculations show that in the oxygen-annealed garnet ceramic $Lu_1Gd_2Ga_3Al_2O_{12}$:Ce 0.2% the $Ce^{4+}$ concentration is 2 ppm. This low $Ce^{4+}$ concentration is sufficient to serve as the dominant electron recombination center because of its Coulomb nature. The effective electron capture radius $r_{RC}$ was determined to be 2.7 Å. For the Coulomb neutral $Yb^{3+}$ electron trap, the effective radius was determined to be much smaller, 0.2 Å. The present results are consistent with earlier observations that small concentrations of divalent cations (e.g., 10−100 ppm $Mg^{2+}$) are sufficient to lead to charge compensation by parts per million levels of $Ce^{4+}$ that significantly speed up decay kinetics[50,51] and reduce afterglow[52] as a result of efficient electron recombination at $Ce^{4+}$ centers.

The present study provides a consistent model describing the electron trapping and recombination in Ce-doped garnets that allows a quantitative description of the time response and afterglow behavior of this important class of materials. The numbers obtained for the capture rates, concentration of $Ce^{4+}$ ions, and recombination cross sections make it possible to simulate the decay kinetics and afterglow of any similar garnet system. The modeling can be utilized to design and optimize luminescent materials based on garnets for application as persistent phosphors, optical converters, or scintillators.



DOI: 10.1021/acs.jpcc.9b05169
J. Phys. Chem. C 2019, 123, 22725−22734

## ■ ASSOCIATED CONTENT

### Supporting Information

The Supporting Information is available free of charge on the ACS Publications website at DOI: 10.1021/acs.jpcc.9b05169.

Details on experimental data, auxiliary estimations, and model calibration (PDF)

## ■ AUTHOR INFORMATION


### Corresponding Author

*E-mail: ivanvrubel@ya.ru.

### ORCID

Ivan I. Vrubel: 0000-0002-8175-0748

Andries Meijerink: 0000-0003-3573-9289


### Notes

The authors declare no competing financial interest.

## ■ ACKNOWLEDGMENTS

I.I.V., R.G.P. and I.A.S. acknowledge support from the Megagrant 14.Y26.31.0015 and Goszadanie no. 3.8884.2017/8.9 of the Ministry of Education and Science of Russian Federation.

## ■ REFERENCES


(1) van Eijk, C. W. E. Inorganic Scintillators in Medical Imaging. *Phys. Med. Biol.* **2002**, *47*, R85.

(2) Xia, Z.; Meijerink, A. Ce3+-Doped Garnet Phosphors: Composition Modification, Luminescence Properties and Applications. *Chem. Soc. Rev.* **2017**, *46*, 275−299.

(3) Ueda, J.; Dorenbos, P.; Bos, A. J. J.; Kuroishi, K.; Tanabe, S. Control of Electron Transfer Between $Ce^{3+}$ and $Cr^{3+}$ in the $Y_3Al_{5-x}Ga_xO_{12}$ Host Via Conduction Band Engineering. *J. Mater. Chem. C* **2015**, *3*, 5642−5651.

(4) Kamada, K.; Endo, T.; Tsutumi, K.; Yanagida, T.; Fujimoto, Y.; Fukabori, A.; Yoshikawa, A.; Pejchal, J.; Nikl, M. Composition Engineering in Cerium-Doped (Lu,Gd)3(Ga,Al)5O12 Single-Crystal Scintillators. *Cryst. Growth Des.* **2011**, *11*, 4484−4490.

(5) Kanai, T.; Satoh, M.; Miura, I. Characteristics of a Non-stoichiometric Gd3+(Al,Ga)5O12:Ce Garnet Scintillator. *J. Am. Ceram. Soc.* **2008**, *91*, 456−462.

(6) Ueda, J.; Kuroishi, K.; Tanabe, S. Bright Persistent Ceramic Phosphors of $Ce^{3+}$-$Cr^{3+}$-codoped Garnet Able to Store by Blue Light. *Appl. Phys. Lett.* **2014**, *104*, 101904.

(7) Nikl, M.; Kamada, K.; Babin, V.; Pejchal, J.; Pilarova, K.; Mihokova, E.; Beitlerova, A.; Bartosiewicz, K.; Kurosawa, S.; Yoshikawa, A. Defect Engineering in Ce-doped Aluminum Garnet Single Crystal Scintillators. *Cryst. Growth Des.* **2014**, *14*, 4827−4833.

(8) Ueda, J.; Hashimoto, A.; Takemura, S.; Ogasawara, K.; Dorenbos, P.; Tanabe, S. Vacuum Referred Binding Energy of 3d Transition Metal Ions for Persistent and Photostimulated Luminescence Phosphors of Cerium-doped Garnets. *J. Lumin.* **2017**, *192*, 371−375.

(9) Selim, F. A.; Varney, C. R.; Tarun, M. C.; Rowe, M. C.; Collins, G. S.; McCluskey, M. D. Positron Lifetime Measurements of Hydrogen Passivation of Cation Vacancies in Yttrium Aluminum Oxide Garnets. *Phys. Rev. B: Condens. Matter Mater. Phys.* **2013**, *88*, 174102.

(10) Van den Eeckhout, K.; Poelman, D.; Smet, P. Persistent Luminescence in non-Eu2+-doped Compounds: a Review. *Materials* **2013**, *6*, 2789−2818.

(11) McKeever, S. W. S. *Thermoluminescence of Solids*; Cambridge Solid State Science Series; Cambridge University Press: New York, 1985.

(12) Pagonis, V.; Kitis, G.; Furreta, C. *Numerical and Practical Exercises in Thermoluminescence*; Springer: New York, 2006.

(13) Chen, R.; Pagonis, V. *Thermally and Optically Stimulated Luminescence: A Simulation Approach*; John Wiley & Sons: New York, 2011.

(14) Abdurazakov, A.; Antonov, V.; Arsen'ev, P. Thermostimulated Luminescence and Thermostimulated Conductivity in Neodymium-doped Yttrium-Aluminum-Garnet Single Crystals. *J. Appl. Spectrosc.* **1982**, *36*, 20−24.

(15) Böhm, M.; Iacconi, P.; Kromm, K.; Scharmann, A. Low Temperature Thermoluminescence and Thermally Stimulated Conductivity in α-Al2O3 Crystals. *Phys. Status Solidi A* **1994**, *146*, 757−764.

(16) Chen, R.; Pagonis, V. On the Expected Order of Kinetics in a Series of Thermoluminescence (TL) and Thermally Stimulated Conductivity (TSC) Peaks. *Nucl. Instrum. Methods Phys. Res., Sect. B* **2013**, *312*, 60−69.

(17) Jackson, J.; Harris, A. The Fading of Optical Absorption Bands in TLD Lithium Fluoride. *Phys. Lett. A* **1969**, *29*, 423−424.

(18) Ueda, J.; Miyano, S.; Tanabe, S. Formation of Deep Electron Traps by Yb3+ Codoping Leads to Super-long Persistent Luminescence in Ce3+-doped Yttrium Aluminum Gallium Garnet Phosphors. *ACS Appl. Mater. Interfaces* **2018**, *10*, 20652−20660 PMID: 29791129. .

(19) Chernenko, K. A.; Mikhrin, S. B.; Wieczorek, H.; Ronda, C. R.; Rodnyi, P. A. Source of Rectangular X-ray Pulses for Studying Scintillators. *Tech. Phys. Lett.* **2015**, *41*, 971−973.

(20) ter Weele, D. N.; Schaart, D. R.; Dorenbos, P. Intrinsic Scintillation Pulse Shape Measurements by Means of Picosecond X-ray Excitation for Fast Timing Applications. *Nucl. Instrum. Methods Phys. Res., Sect. A* **2014**, *767*, 206−211.

(21) Nikl, M.; Vedda, A.; Laguta, V. Energy Transfer and Storage Processes in Scintillators: The Role and Nature of Defects. *Radiat. Meas.* **2007**, *42*, 509−514 Proceedings of the 6th European Conference on Luminescent Detectors and Transformers of Ionizing Radiation (LUMDETR 2006). .

(22) Moretti, F.; Patton, G.; Belsky, A.; Fasoli, M.; Vedda, A.; Trevisani, M.; Bettinelli, M.; Dujardin, C. Radioluminescence Sensitization in Scintillators and Phosphors: Trap Engineering and Modeling. *J. Phys. Chem. C* **2014**, *118*, 9670−9676.

(23) Blasse, G.; Bril, A. A New Phosphor for Flying-Spot CathodeRay Tubes for Color Television: YellowEmitting Y3Al5O12Ce3+. *Appl. Phys. Lett.* **1967**, *11*, 53−55.

(24) Nikl, M.; Babin, V.; Mares, J.; Kamada, K.; Kurosawa, S.; Yoshikawa, A.; Tous, J.; Houzvicka, J.; Blazek, K. The Role of Cerium Variable Charge State in the Luminescence and Scintillation Mechanism in Complex Oxide Scintillators: The Effect of Air Annealing. *J. Lumin.* **2016**, *169*, 539−543 The 17th International Conference on Luminescence and Optical Spectroscopy of Condensed Matter (ICL'14). .

(25) Gundacker, S.; Turtos, R.; Auffray, E.; Lecoq, P. Precise Rise and Decay Time Measurements of Inorganic Scintillators by Means of X-ray and 511 keV Excitation. *Nucl. Instrum. Methods Phys. Res., Sect. A* **2018**, *891*, 42−52.

(26) Robbins, D.; Cockayne, B.; Glasper, J.; Lent, B. The Temperature Dependence of Rare-Earth Activated Garnet Phosphors I. Intensity and Lifetime Measurements on Undoped and Ce-doped. *J. Electrochem. Soc.* **1979**, *126*, 1213−1220.

(27) Xia, Z.; Meijerink, A. Ce3+-Doped Garnet Phosphors: Composition Modification, Luminescence Properties and Applications. *Chem. Soc. Rev.* **2017**, *46*, 275−299.

(28) Liu, S.; Feng, X.; Zhou, Z.; Nikl, M.; Shi, Y.; Pan, Y. Effect of Mg2+ Co-doping on the Scintillation Performance of LuAG:Ce Ceramics. *Phys. Status Solidi RRL* **2014**, *8*, 105−109.

(29) Drozdowski, W.; Brylew, K.; Witkowski, M.; Wojtowicz, A.; Solarz, P.; Kamada, K.; Yoshikawa, A. Studies of Light Yield as a Function of Temperature and Low Temperature Thermoluminescence of Gd3Al2Ga3O12:Ce Scintillator Crystals. *Opt. Mater.* **2014**, *36*, 1665−1669 SI: IWASOM'13. .

(30) Mihokova, E.; Nikl, M.; Mares, J.; Beitlerova, A.; Vedda, A.; Nejezchleb, K.; Blazek, K.; D'Ambrosio, C. Luminescence and




DOI: 10.1021/acs.jpcc.9b05169
J. Phys. Chem. C 2019, 123, 22725−22734

Scintillation Properties of YAG:Ce Single Crystal and Optical Ceramics. *J. Lumin.* **2007**, *126*, 77−80.
(31) Khanin, V. M.; Rodnyi, P. A.; Wieczorek, H.; Ronda, C. R. Electron Traps in Gd3Ga3Al2O12:Ce Garnets Doped with Rare-earth Ions. *Tech. Phys. Lett.* **2017**, *43*, 439−442.
(32) Khanin, V.; Venevtsev, I.; Rodnyi, P.; Ronda, C. Changes in Trap Parameters in Various mixed Oxide Garnets. *Radiat. Meas.* **2016**, *90*, 104−108.
(33) Sunta, C. *Unraveling Thermoluminescence*; Springer: New York, 2015.
(34) Khanin, V. M.; Vrubel, I. I.; Polozkov, R. G.; Shelykh, I. A.; Venevtsev, I. D.; Meijerink, A.; Wieczorek, H.; Boerekamp, J.; Spoor, S.; Rodnyi, P. A.; Ronda, C. Modeling and Assessment of Afterglow Decay Curves from Thermally Stimulated Luminescence of Complex Garnets. *J. Phys. Chem. A* **2019**, *123*, 1894−1903.
(35) Brylew, K.; Drozdowski, W.; Wojtowicz, A. J.; Kamada, K.; Yoshikawa, A. Studies of Low Temperature Thermoluminescence of GAGG:Ce and LuAG:Pr Scintillator Crystals Using the TmaxTstop Method. *J. Lumin.* **2014**, *154*, 452−457.
(36) Gektin, A. V.; Belsky, A. N.; Vasil'ev, A. N. Scintillation Efficiency Improvement by Mixed Crystal Use. *IEEE Trans. Nucl. Sci.* **2014**, *61*, 262−270.
(37) Belsky, A.; Gektin, A.; Gridin, S.; Vasil'ev, A. N. Electronic and Optical Properties of Scintillators Based on Mixed Ionic Crystals. *Springer Proc. Phys.* **2017**, *200*, 63−82.
(38) Feofilov, S.; Kulinkin, A.; Ovanesyan, K.; Petrosyan, A. Discrete Zero-phonon Cr3+ Lines in the Spectra of TerbiumYttriumLutetium Aluminum Garnets Solid Solutions: Lattice Compression and Dilation. *Solid State Commun.* **2016**, *226*, 39−43.
(39) Laguta, V.; Zorenko, Y.; Gorbenko, V.; Iskaliyeva, A.; Zagorodniy, Y.; Sidletskiy, O.; Bilski, P.; Twardak, A.; Nikl, M. Aluminum and Gallium Substitution in Yttrium and Lutetium AluminumGallium Garnets: Investigation by Single-crystal NMR and TSL Methods. *J. Phys. Chem. C* **2016**, *120*, 24400−24408.
(40) Fasoli, M.; Vedda, A.; Nikl, M.; Jiang, C.; Uberuaga, B. P.; Andersson, D. A.; McClellan, K. J.; Stanek, C. R. Band-gap Engineering for Removing Shallow Traps in Rare-earth $Lu_3Al_5O_{12}$ Garnet Scintillators Using $Ga^{3+}$ Doping. *Phys. Rev. B: Condens. Matter Mater. Phys.* **2011**, *84*, 081102.
(41) Nikl, M.; Mihokova, E.; Pejchal, J.; Vedda, A.; Zorenko, Y.; Nejezchleb, K. The Antisite LuAl Defect-related Trap in Lu3Al5O12:Ce Single Crystal. *Phys. Status Solidi B* **2005**, *242*, R119−R121.
(42) Ueda, J.; Dorenbos, P.; Bos, A. J. J.; Meijerink, A.; Tanabe, S. Insight into the Thermal Quenching Mechanism for Y3Al5O12:Ce3+ Through Thermoluminescence Excitation Spectroscopy. *J. Phys. Chem. C* **2015**, *119*, 25003−25008.
(43) Luo, Y.; Xia, Z. Effect of Al/Ga Substitution on Photoluminescence and Phosphorescence Properties of Garnet-Type Y3Sc2Ga3xAlxO12:Ce3+ Phosphor. *J. Phys. Chem. C* **2014**, *118*, 23297−23305.
(44) Wu, H.; Yang, C.; Zhang, Z.; Tang, Y. Photoluminescence and Thermoluminescence of Ce3+ Incorporated Y3Al5O12 Synthesized by Rapid Combustion. *Optik* **2016**, *127*, 1368−1371.
(45) Lucchini, M.; Babin, V.; Bohacek, P.; Gundacker, S.; Kamada, K.; Nikl, M.; Petrosyan, A.; Yoshikawa, A.; Auffray, E. Effect of Mg2+ Ions Co-doping on Timing Performance and Radiation Tolerance of Cerium Doped Gd3Al2Ga3O12 Crystals. *Nucl. Instrum. Methods Phys. Res., Sect. A* **2016**, *816*, 176−183.
(46) Wu, Y.; Meng, F.; Li, Q.; Koschan, M.; Melcher, C. L. Role of $Ce^{4+}$in the Scintillation Mechanism of Codoped.:$Gd_3Ga_3Al_2O_{12}$,Ce. *Phys. Rev. Appl.* **2014**, *2*, 044009.
(47) Liu, S.; Mares, J. A.; Feng, X.; Vedda, A.; Fasoli, M.; Shi, Y.; Kou, H.; Beitlerova, A.; Wu, L.; D'Ambrosio, C.; Pan, Y.; Nikl, M. Towards Bright and Fast Lu3Al5O12:Ce,Mg Optical Ceramics Scintillators. *Adv. Opt. Mater.* **2016**, *4*, 731−739.
(48) Sunta, C. M.; Kulkarni, R. N.; Yoshimura, E. M.; Mol, A. W.; Piters, T. M.; Okuno, E. Interactive Kinetics in Thermoluminescence (TL) and Its Effect on Glow Curves and Their Growth as a Function of Dose. *Phys. Status Solidi B* **1994**, *186*, 199−208.
(49) Muñoz-García, A. B.; Anglada, E.; Seijo, L. First-principles Study of the Structure and the Electronic Structure of Yttrium Aluminum Garnet Y3Al5O12. *Int. J. Quantum Chem.* **2009**, *109*, 1991−1998.
(50) Prusa, P.; Kucera, M.; Babin, V.; Bruza, P.; Panek, D.; Beitlerova, A.; Mares, J. A.; Hanus, M.; Lucenicova, Z.; Nikl, M. Garnet Scintillators of Superior Timing Characteristics: Material, Engineering by Liquid Phase Epitaxy. *Adv. Opt. Mater.* **2017**, *5*, 1600875.
(51) Sidletskiy, O.; Lebbou, K.; Kofanov, D.; Kononets, V.; Gerasymov, I.; Bouaita, R.; Jary, V.; Kucerkova, R.; Nikl, M.; Polesel, A.; Pauwels, K.; Auffray, E. Progress in Fabrication of Long Transparent YAG:Ce and YAG:Ce,Mg Single Crystalline Fibers for HEP Applications. *CrystEngComm* **2019**, *21*, 1728−1733.
(52) Schauer, P.; Lalinsky, O.; Kucera, M.; Lucenicova, Z.; Hanus, M. Effect of Mg Co-doping on Cathodoluminescence Properties of LuGAGG:Ce Single Crystalline Garnet Films. *Opt. Mater.* **2017**, *72*, 359−366.


DOI: 10.1021/acs.jpcc.9b05169
*J. Phys. Chem. C* 2019, 123, 22725−22734